Energy-Efficient Service-Aware Multi-Connectivity Scheduler for Uplink Multi-Layer Non-Terrestrial Networks

Michael N. Dazhi, *Graduate Student Member, IEEE*, Hayder Al-Hraishawi, *Senior Member, IEEE*, M. R. Bhavani Shankar, *Senior Member, IEEE*, Symeon Chatzinotas, *Fellow, IEEE*, and Björn Ottersten, *Fellow, IEEE*

***Abstract*—This paper introduces the concept of energy efficiency (EE) in the uplink with the capability of multi-connectivity (MC) in a multi-orbit non-terrestrial network (NTN), where user terminals (UTs) can be simultaneously served by more than one satellite to achieve higher peak throughput at reduced energy consumption. This concept also considers the service classification of the users, so that network dimensioning is performed in order to satisfy the quality of service (QoS) requirement of users. MC can increase throughput, but this entails increased power consumption at user terminal for uplink transmissions. To this end, an energy-efficient service-aware multi-connectivity (EE-SAMC) scheduling algorithm is developed in this paper to improve the EE of uplink communications. EE-SAMC uses available radio resources and propagation information to intelligently define a dynamic resource allocation pattern, that optimally routes traffic so as to reduce the energy consumption at the UT while ensuring QoS is maximized. EE-SAMC is designed based on the formulation of a non-convex combinatorial problem, it is solved in two ways involving firstly an optimization solution and secondly a heuristic approach. The effectiveness of EE-SAMC is compared with random allocation, round robin and heuristic schedulers in terms of EE, throughput and delay; EE-SAMC outperforms all schedulers.**

***Index Terms*—Energy efficiency, green communication, multi-connectivity, non-terrestrial network (NTN), resource allocation, satellite communications, scheduling.**

I. Introduction

ENERGY efficiency is a growing concern in the design of satellite networks and there are concerted efforts to reduce the energy consumption of satellite communication systems, especially in the ground segment [1], [2]. Most satellite user terminals (UTs) have been traditionally designed to operate on an always-on basis, which can result in significant energy usage [3]. This impact is becoming more significant as the number of UTs increases, resulting in elevated levels of carbon dioxide (CO_2) emissions and raising environmental issues. To mitigate these concerns, it is crucial to focus on efficient uplink transmissions and to implement power-saving measures wherever possible [4]. Consequently, employing such procedures can reduce the environmental footprint of satellite communication systems while maintaining global connectivity that is both reliable and effective. This underscores the importance of considering the EE of satellite networks and making it a priority in their design and operation. Thus, the escalating energy costs and the associated global carbon emissions from the communications devices have inspired researchers to devote more efforts for developing energy-efficient communication systems [5].

Furthermore, satellite communications industry is witnessing a major transformation because the paradigm shift brought about by several key technological advancements such as software-defined satellites, very high throughput satellites (VHTS), non-geostationary orbit (NGSO) systems, virtualization and service orchestration [6]. Specifically, recent developments primarily focus on deploying reconfigurable satellite payloads in order to offer generic and software-based solutions as well as providing high throughput transmissions [7]. In addition to the established satellite applications like aeronautical, maritime, mapping, weather forecasting, and broadcasting, the recent advances have opened up the satellite potentials to convey and execute various innovative use cases and new services from space [8]. Therefore, satellite traffic demand is currently soaring to provide affordable, accessible, uninterrupted wireless connectivity especially to the underserved and unserved areas.

Another hurdle faced by the satellite communications is the scarcity of resources particularly the radio frequency (RF) spectrum [9]. Therefore, it is crucial to devise unconventional techniques to improve resource utilization while satisfying the high data rate and low latency requirements. In this direction, an intriguing concept has been recently studied within the multi-beam satellite architectures, that is dual connectivity (DC), which allows users to be simultaneously served with different systems and/or frequency bands [10]. The DC feature has been considered by the 3rd Generation Partnership Project (3GPP) in Release 12 for adoption to the fifth-generation (5G) New Radio (NR) specifications owing to its capability of

Manuscript received 29 November 2022; revised 12 March 2023; accepted 13 April 2023. Date of publication 21 April 2023; date of current version 21 August 2023. This work was supported by Fond National de la Recherche (FNR) under the Industrial Partnership Block Grant (IPBG) through the Project INSTRUCT: Integrated Satellite—TeRrestrial Systems for Ubiquitous Beyond 5G Communications Networks under Grant 14016225. This work in part has been presented at IEEE Global Communications Conference (GLOBECOM) 2022, Brazil [DOI: 10.1109/GCWkshps56602.2022.10008521]. The editor coordinating the review of this article was F. Yang. *(Corresponding author: Michael N. Dazhi.)*

The authors are with the Interdisciplinary Centre for Security, Reliability and Trust, University of Luxembourg, 1855 Luxembourg City, Luxembourg (e-mail: michael.dazhi@uni.lu).

Digital Object Identifier 10.1109/TGCN.2023.3269283

maximizing the spectrum utilization and avoiding the traffic overload [11]. Similarly, the well-known carrier aggregation (CA) concept has been introduced to the satellite communication systems [12] to increase the achievable peak data rate, where a single user is served by multiple beams/carriers simultaneously.

Beyond this, multi-layered non-terrestrial network (NTN) is a vital enabler for providing ubiquitous and ultra-high capacity global connectivity to a wide range of applications requiring high availability and high resilience [13]. Multi-layered multi-orbit hierarchical NTNs of satellites, i.e., the orchestration among different satellites cooperating at different altitudes, are a highly appealing technological solution for addressing coverage and latency constraints associated with the NTN paradigm. In this direction, the 3GPP group has lately codified the use of satellites and aerial platforms to construct multi-layer NTNs in order to provide space-based 5G communication services and support future wireless ecosystems [14]. Thus, it is essential to expand the concept of DC into MC in order to adapt to the flexibility and scalability offered by the emerging NTN architectures and the integrated terrestrial and non-terrestrial communication systems [15], [16].

The MC techniques are envisioned as an indispensable technology to significantly enhance the offered system capacity and improve the spectral efficiency in the heterogeneous networks. An important foreseeable application of MC is the interworking among various communication standards and architectures promoting a smoother transition, e.g., between fourth generation (4G) and 5G systems [17]. The MC solution achieves not only higher per-user data rate but also provides mobility robustness, and thus, it can improve the resilience of wireless communications [18]. Additionally, data traffic in NTNs is highly diverse and randomly distributed in the service areas, and arising from various users with different quality-of-service (QoS) requirements [19]. Thus, employing MC in NTNs would help satisfy the asymmetry and heterogeneity of traffic demands. However, enabling MC in UTs to utilize multiple aggregated carriers/systems that inevitably comes at the cost of higher power consumption [12]. Further, the EE in NTNs is one of the major challenges, especially for uplink transmissions and for the battery-limited mobile terminals [20].

In the literature, some contributions have studied and evaluated the issue of EE for the uplink transmissions in the satellite domain. For instance, the energy resource allocation problem in the uplink communications is investigated in [21] within the space-air-ground Internet of Remote Things networks, which aims at maximizing the system EE by jointly optimizing sub-channel selection and uplink transmission power control. In [22], a joint optimization model of spectrum efficiency and EE in a single-station multi-satellite multiple input multiple output (MIMO) system was proposed based on a knee-point driven optimization algorithm. Further, a spatial group based optimal uplink power control scheme is proposed in [23] for enhancing the performance of random access in satellite networks. Additionally, two optimal power control schemes are proposed in [24] for maximizing both delay-limited capacity and outage capacity in cognitive satellite terrestrial networks, which are useful performance indicators for real-time applications. It is worth noting that the aforementioned works [21], [22], [23], [24] do not consider concurrent aggregating multi-orbit scenarios in optimizing the uplink transmit power for satellite users.

Nevertheless, the potential of performance enhancements in throughput, latency, and reliability with MC especially for the new service use-cases of 5G [25], [26], have motivated this work to further investigate the uplink EE issue from a UT standpoint. Furthermore, network resiliency and redundancy is an important feature that empowers the network high survivability in the event of failures, and multi-layer architecture is a promising technology that is going to be explored in this direction [27]. The power limitation of UTs including the battery-powered which are sometimes used in remote/rural areas [28], is a fundamental problem that requires intervention; this is the focus of this paper. Similarly the global CO_2 emission reduction target of 45% by 2030 and carbon neutrality by 2050 [29] is also a motivation to investigate ways to enhance the EE of the ever-increasing satellite users. To the best of our knowledge, optimizing the uplink transmit power problem has not been studied yet in the open literature within MC enabled multi-orbit NTNs. In addition, a novel scheduling technique is proposed to satisfy the variations in user traffic demand.

Contributions: Our key technical contributions can be explicitly summarized as follows:

1) Design guidelines are outlined for the deployment of a multi-layer satellite network comprising low earth orbit (LEO), medium earth orbit (MEO), and geostationary earth orbit (GEO) satellites, which are all served by multi-orbital hybrid gateway stations (HGSs) [10]. These gateway stations operate with softwarized controller and network function virtualization (NFV) elements at the network and data link layers, the softwarized controller performs functions including the segmentation and classification of protocol data units (PDUs) based on the service category of the transmitting user [1]; this allows for a pure softwarized implementation of schedulers. PDUs are specific block of information units transmitted over a network channel.
2) Developing a scheduler aided by a segmentation algorithm with protocol stack adaptation, which assigns priority and preference for resource allocation to PDUs based on identified service classes. In this work, three classes are considered from 3GPP; namely, ultra-reliable low latency communication (URLLC),[1] massive machine type communication (mMTC), and enhanced mobile broadband (eMBB).
3) An energy-efficient service aware multi-connectivity (EE-SAMC) scheduling algorithm is developed for optimal resource allocation involving power and spectrum leading to a high capacity transmission with energy efficiency in the uplink. This algorithm considers radio parameters such as transmit power, carrier-to-noise ratio

[1]3GPP requirements for URLLC cannot be satisfied in satellite communications due to propagation delay, so this represents latency-sensitive traffic/services in this paper.

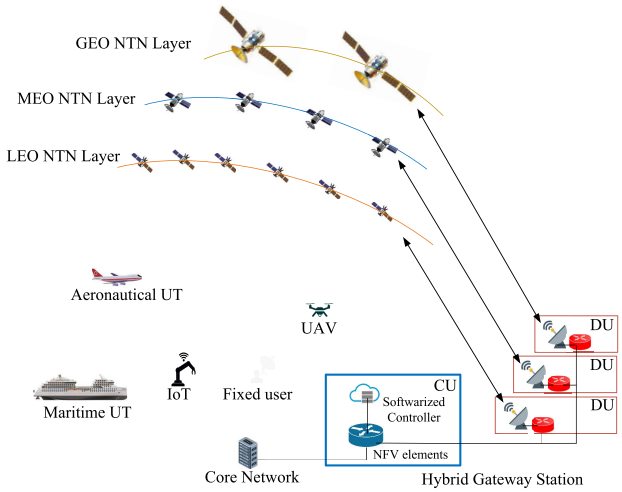

Fig. 1. A schematic diagram of the network topology for the multi-layer NTN.

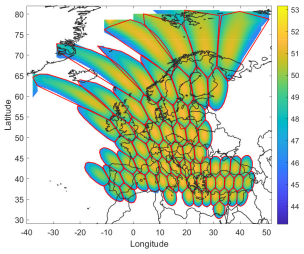

(a) The 71 beam pattern of ESA over Europe.

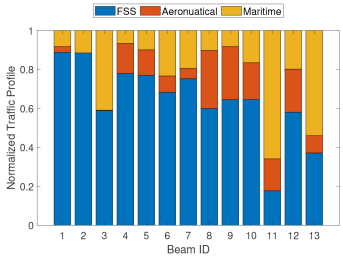

(b) Traffic profile of heterogeneous demand with 71 beam pattern.

Fig. 2. Emulated heterogeneous traffic for FSS, aeronautical and maritime over the European continent [19].

(*C/N*) and the energy-per-bit-to-noise ratio (E_b/N_o) of the available orbital satellite links. Scheduling and resource allocation are performed jointly.

4) The service aware multi-connectivity (SAMC) heuristic scheduler is designed based on 3GPP specification and link budget analysis. The proposed EE-SAMC algorithm and heuristic scheduler are evaluated by simulations and then compared to other state-of-the-art algorithms in terms of throughput, delay and energy efficiency.

The rest of the paper is structured as follows. In Section II, the network model and architecture are extensively discussed. The following Section III focuses on the resource allocation optimization problem. In Section IV, the proposed solution for the optimization problem is outlined. While the simulation setup and performance evaluation are covered in Section V. Finally, the conclusion and future work are summarised in Section VI.

II. Network Model and Architecture

A. Network Topology and Service Architecture

The network topology consists of the three layers of LEO, MEO and GEO satellite constellations, along with a HGS in which resides NFV elements with softwarized controllers at the central unit (CU), that controls the communication to these satellites through multiple inter-connected antenna ports operating in their respective distributed unit (DU), as shown in Fig. 1. The corresponding satellites then configure beams which provide coverage to various UT types such as terrestrial fixed, maritime, aeronautical, land-mobile, and Internet of Things (IoT). Fig. 2 shows a representation for fixed satellite service (FSS), aeronautical, and maritime heterogeneous traffic demand over the European continent from the coverage of 71 beam pattern provided by the European space agency (ESA) [19]. This clearly shows the dynamic service requirements involving different terminals with different service demands in the same geographical area. For instance, the traffic demands in the beam range from the 4*th* to the 13*th* beam is widely diverse in terms of type and amount as shown in Fig. 2 (b). The HGS is configured with network elements (NEs) including NFV elements and softwarized controller operating at the network and data link layers. The softwarized segmentation unit (SSU) is in the NFV element, which performs the segmentation and classification of PDUs into different queues based on the service class demand of the user. This action allows the scheduling algorithm to allocate resources efficiently with high flexibility thereby optimizing the network key performance indicators (KPIs).

The proposed multi-layer NTN resource scheduling architecture is shown in Fig. 3, both control and user plane structural designs are provided along with the protocol stack of the open system interconnect layers and corresponding 5G sublayers as described in [30]. In the control plane, some of the signaling activities that occur between the UT, radio access network (RAN), and core network (CN) include link adaptation, UT authentication, scheduling request and others. Link adaptation is performed at the physical layer, where the UT sends the estimated channel state to the HGS to perform the adaptation of modulation, coding and power. The UT also sends non access stratum (NAS) protocol signaling messages from the network layer to the CN, this message is passed transparently through the RAN, NAS is used for authentication of UT in the network. The service class of the UT is also determined from the service identification (SID) in the signaling message, and this is sent to the SSU in the radio link control (RLC) sublayer for classification and segmentation definitions. When the UT sends the scheduling request to the HGS from the medium access control (MAC) sublayer of the data link layer, the HGS will use the classification information from the SSU, to schedule and map the appropriate resources that meet the QoS requirement of the service class of the UT, this is done by using the radio scheduler (RS)

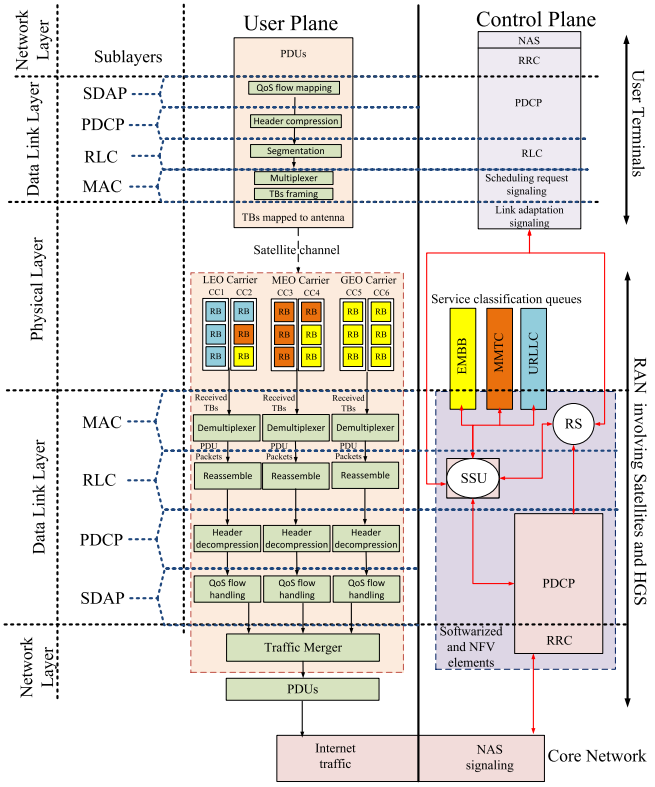

Fig. 3. Schematic diagram of service aware multi-layer NTN resource scheduling architecture for the uplink transmission scenario.

and the proposed algorithm running in it at the MAC sublayer. The radio resource controller (RRC) sublayer handles the RRC connection establishment, maintenance and release signaling between the UT and HGS, where the addition, modification and release of CA, DC and MC is initiated.

In the user plane, PDUs from the network layer of the UT are transfer to the service data adaptation protocol (SDAP) sublayer in the data link layer, where QoS flow mapping is performed onto data radio bearers for each PDU session. This is further sent to the packet data convergence protocol (PDCP) sublayer, where header compression and ciphering is performed on the PDUs. At the RLC sublayer, segmentation is performed on the PDUs, and then the PDUs are forwarded to the multiplexer in the MAC sublayer, where the PDUs are multiplexed and mapped from logical channels to transport channels. Then framing into transport blocks (TBs) occurs, and the TBs are mapped to the antenna in the PHY layer, then transmitted using appropriate satellites (either LEO, MEO or GEO), component carriers (CCs) and resource block (RBs) in PHY of the HGS, based on the scheduling pattern assign by RS inline with the service classification of SSU identified during the signaling session on the control plane. The TBs of different UTs in the uplink direction follow a Markovian arrival process with arrival rate *A* [31], arrive at the demultiplexer unit in the MAC sublayer, where TB frames are demultiplexed to PDUs, belonging to one or more logical channels from transport channels of physical layer. Then MAC pass the PDUs to the reassemble unit of the RLC sublayer for reassembling. Header decompression and deciphering is performed at the PDCP sublayer on the PDUs. Furthermore, the PDCP then pass the PDUs to the SDAP sublayer for QoS flow handling after which the PDUs are merged at the traffic merger in the network layer and pass to the CN as Internet traffic. It is important to note that SDAP protocol only exits in the user plane and it does not exit in the control plane. Based on our proposed architecture, the datalink and network layer parts of the HGS are softwarized and NFV elements. This virtualisation at the HGS, will introduce energy consumption reduction at the HGS as fewer physical network elements will be required to function for the three orbitals as compared to conventional gateway stations [32].

As the scheduling algorithm is executed in the RS unit, it implements the resource allocation process based on input radio link parameters including transmit power (P_{tx}), uplink *C/N*, and the E_b/N_o along with the information of the type of service required by the uplink transmitting terminal in the control plane. In this paper, three service classes are considered in the optimization problem of the proposed EE-SAMC scheduling algorithm, i.e., URLLC, mMTC, and eMBB as detailed in 3GPP Release-15 of 5G standards [14]. The following conditions must be satisfied to perform the dynamic resource allocation and traffic steering using the EE-SAMC algorithm.

- There must be sufficient E_b/N_o value to satisfy the link budget requirement for the respective LEO, MEO, and GEO satellite links.
- The orbital satellites of LEO, MEO, and GEO must be visible to the users employing MC. In addition, the UTs must be capable of connecting to the three orbital constellations [33].
- The UTs must be capable of informing the HGS of its unique service category with a SID via signalling information exchange, which will allow the SSU at the HGS to differentiate UTs into the different service classes. This can be done by implementing policy control configurations with stored subscription information of the users in a subscriber database.

B. Uplink Transmission Model

The uplink transmission begins from the UT that transmits to the satellites in the constellation, then further to the HGS which is connected to the core network, the satellite and the HGS comprise of the RAN. The communication link is established based on the ink budget analysis with air-interface configurations that accounts for the required power and gains to successfully transmit over the satellite channel. The total path losses (*PL*) in dB of the link between the UT and the satellite can be modelled as follow:

$$PL = FSL + L_{atm} + L_s + L_\sigma \tag{1}$$

where *FSL* is the free space loss that is given in (2). The atmospheric loss (L_{atm}) accounts for the losses from the atmosphere, which is modelled by taking into consideration temperature, pressure, and water vapour density as provided in ITU-R P.676 [34]. The signal loss due to tropospheric or ionospheric scintillation is represented as L_s which impacts signals

TABLE I
LIST OF USED SYMBOLS

Symbol	Definition	Symbol	Definition
P_{tx}, P_{tx}^U, P_i	Transmit power	$\vartheta_i(t, F_c)$	Channel gain
C/N	Carrier to noise ratio	Y, y	Number of propagation paths
E_b/N_o	Energy per bit to noise ratio	R, R	Achievable rate
PL, PL_{t,S_t}	Total path loss	ρ	Traffic/system load
FSL	Free space loss	μ	Processing service time
L_{atm}	Atmospheric loss	A	Arrival rate
L_s	Loss due to troposheric or ionospheric scintillation	E_{η_i}, E	Energy efficiency
L_σ	Zero mean lognormal variable of shadowing environment	ϕ_i	Service class
F_c	Carrier frequency	s, S	Number of satellites
D	Propagation distance	P_c	UT circuitry power consumption
C_{pi}^U	Satellite received carrier power	a, b, c	URLLC, mMTC, eMBB
$EIRP_i^U$	Uplink EIRP of UT	M	Number of allowable CCs
G_{Si}	Satellite antenna gain	Z	Number of allowable satellites
G_{tx}^U	UT antenna gain	R_i^{min}	Minimum allowable data rate
N	Noise power	P_i^{max}	Maximum allowable transmit power
k_B	Boltzmann's constant	D_i^{max}	Maximum allowable latency
T	Noise temperature	ξ	Barrier parameter
B	Bandwidth	v, v_i	Slack variables
I_i^U	Uplink interference	$L(p, \lambda)$	Lagrange function
C/I	Carrier to interference ratio	$f_\xi(p, v)$	Merit function
γ_i^U	Carrier to interference and noise ratio	λ_g	Lagrange multiplier
t	time	H	Hessian
$\varrho_i(t, F_c)$	Space domain channel response	D_i	Latency
φ_i	Doppler shift	α, α_k^i	Weighting factor
τ_i	Propagation delay	η	Energy efficiency objective function
k, K	Number of resource blocks	C_t	Entropy penalty constant
i, I	Number of UTs	J	Jacobian
j, J	Number of component carriers	e	Vector of ones
$Q_{i,s,j,k}$	Independent variable indicator	G'	Weighted bipartite graph
c	Number of servers	M_p^*, M_p	Perfect matching

in Ka band, and this is influenced by the user elevation angle as described in ITU-R P.618 [35]. L_σ represents zero mean lognormal variable with variance indicating the harshness of shadowing environment $L_\sigma \sim (0, \sigma^2)$, where σ^2 values are given by 3GPP for rural, dense urban and urban scenarios [36].

$$FSL = 32.45 + 20\log_{10} F_c + 20\log_{10} D \tag{2}$$

where F_c is the carrier frequency in GHz and *D* is the propagation distance in meters. In this system, the UTs are randomly distributed within the coverage area of the satellites, and the impact of the inter-user interference is taken into account. Specifically, an intended UT_i is served by the satellite S_i while interfering UT_t is served by interfering beam of another satellite S_t. Then, the received power at the satellite S_i from UT_i is computed as follows

$$C_{pi}^U = EIRP_i^U + G_{S_i} - PL \tag{3}$$

where the uplink $EIRP_i^U$ is based on the radiation pattern of the UT antenna and expressed as $EIRP = P_{tx}^U + G_{tx}^U$, with P_{tx}^U and G_{tx}^{UT} representing transmit power in dB and gain in dBi of the UT. G_{S_i} is the gain of the satellite S_i. The uplink noise power is expressed as:

$$N = 10\log_{10}(k_B\, TB) \tag{4}$$

where k_B is the Boltzmann's constant in J/K, *T* is equivalent noise temperature of the satellite antenna in Kelvin and *B* is the bandwidth in Hz.

Thereby, the uplink *C/N* in dB is obtained by subtracting (4) from (3) in dB as shown below:

$$C/N_i^U = EIRP_i^U + G_{S_i} - PL - N \tag{5}$$

Consequently, the total interference in the uplink (I_i^U) in dB is derived as:

$$I_i^U = EIRP_t^U + G_{S_t} - PL_{t,S_t} \tag{6}$$

This is the interference from UT_t served by satellite S_t. The resultant carrier to interference ratio (*C/I*) in dB is given as

$$C/I_i^U = EIRP_i^U + G_{S_i} - PL - I_i^U \tag{7}$$

The carrier to interference and noise ratio (*C/I* + *N*) in dB is [36]:

$$\gamma_i^U = C/I + N_i^U = -10\log_{10}\left(10^{-0.1C/N_i^U} + 10^{-0.1C/I_i^U}\right) \tag{8}$$

- *Uplink Channel Model:* The uplink channel can be modeled as a ray-tracing channel modeling approach. Using this approach, the space domain channel response between UT *i* and satellite *s* at time *t* and frequency F_c is represented as [37]

$$\varrho_i(t, F_c) = exp\{j2\pi[t\varphi_i - F_c\tau_i]\} \cdot \vartheta_i(t, F_c) \tag{9}$$

where *j* is $\sqrt{-1}$, φ_i is Doppler shift, τ_i is propagation delay and $\vartheta_i(t, F_c)$ is the UL channel gain of the UT *i*

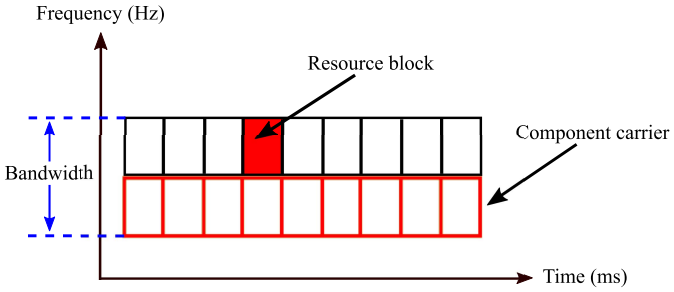

Fig. 4. Resource block and component carrier.

given as

$$\vartheta_i(t, F_c) \triangleq \sum_{y=1}^{Y-1} \vartheta_i . exp\{j2\pi[t\varphi_i - F_c\tau_i]\} \quad (10)$$

where Y is the number of propagation paths of the UT i. The channel model in (9) is applicable when the relative position of the UT and satellite do not change substantially. If the UT and/or the satellite move over wide distances, the channel parameters mentioned above will vary and they will require to be update accordingly [38].

- *Radio Resource:* This is the radio resources used for scheduling, it comprises CCs that are made up of several RBs that serve as time and frequency domain resources as shown in Fig. 4.
- *Achievable Rate:* Assuming ideal HGS to satellite links, the achievable rate in Mbps on the return link of UT_i though satellite S_i on RB k and CC j with bandwidth B is

$$\bar{R} = B \log_2\left(1 + \gamma_i^{UT}\right) \quad (11)$$

Hence the average data rate is expressed as

$$R_i = \sum_{j=1}^{J} \bar{R}_{ij} \quad (12)$$

where the number of CCs is represented by J.

- *System Queuing Model:* The satellite UL PDU transmission can be modelled with *M*/*M*/*c*-PS queue model, where the first M is for the Markovian Poisson arrival and the second M represents the exponentially distributed service time in a processor sharing (PS) having c servers [39]. Here the UTs transmit the PDUs which arrive the RAN in a Markovian arrival process with A arrival rate, and PDU process service time as μ at the server. The system load is given as [40]:

$$\rho = \frac{A}{c.\mu} \quad (13)$$

- *5G Service Classification:* The service classification adopted includes URLLC, mMTC and eMBB as specified by 3GPP.
  - URLLC application services are latency intolerant such as industrial automation and smart grids, hence network dimensioning is performed to satisfy the objective of low latency transmission, which can be achieved with LEO resource. Although LEO cannot guarantee the 3GPP requirements, it will be used for URLLC because it exhibits the lowest latency.
  - mMTC use case involves IoT which requires low power consumption for many connected devices; continuity of service for telematic applications of a group of sensor devices distributed over stationary or mobile wide areas, examples of mMTC applications includes assets tracking and surveillance of critical oil infrastructure. This particular service class has a characteristic of limited power budget for signal transmission especially in the uplink, hence LEO and MEO can be used for resource scheduling.
  - The eMBB service class requires high data rate resilience transmission network with high traffic capacity, and majority of the traffic demand is less sensitive to delay. Examples of eMBB use case includes provisioning of broadband connectivity to passengers on board a cruise ship and TV/multimedia service delivery to homes [14]. Hence LEO, MEO and GEO resources can be used even in DC/MC for this service.

C. Energy Efficiency Metrics

The achievable energy efficiency in a transmission system is the ratio of data rate R to the transmission power P required to achieve R [31]. It is expressed in bits-per-Joules (b/J) as given in (14).

$$E = \frac{R}{P(R)} = \frac{B \log_2\left(1 + \frac{P_{tx}^U G_{tx}^U G_{S_i} PL}{k_B TB}\right)}{P_{tx}^U + P_c} \quad (14)$$

where P_c is UT circuitry power consumption [41].

III. Resource Allocation Optimization Problem

A. The Objective Function

The energy efficiency of the users is defined as

$$\max_{Q_{i,s,j,k} P_i} \sum_{i=1}^{I} \sum_{s=1}^{S} \sum_{j=1}^{J} \sum_{k=1}^{K} \phi_i E_{\eta_i} Q_{i,s,j,k} \quad (15)$$

where $E_{\eta_i} = \frac{R_i}{P_i(R_i)}$ is the energy efficiency of UT_i with R_i and $P_i(R_i)$ as the data rate and transmit power, respectively. Additionally, $Q_{i,j,k,s}$ is an independent variable that denotes UT_i can be scheduled on the k-th *RB* of the j-th CC on satellite s. Further, ϕ_i is the traffic class connection identifier of the UT_i and $\phi_i \in \{a, b, c, 0\}$ which allows the resource allocation algorithm to give different resource priority and allocation preference to different users based on their service classes; i.e., a, b or c that correspond to URLLC, mMTC and eMBB, respectively.

B. Optimization Constraints

The design of the EE-SAMC strategy will be subject to several key constraints as detailed next.

1) Constraint on Route Selection: The PDUs can only be transmitted through available RBs on CCs of satellites, hence, the route selection strategy should be subjected to the utilization of these resources and service identity of the user.

$$\mathbb{C}_1 : \sum_{i=1}^{I} Q_{i,s,j,k} \leq 1 \quad \forall k \in K, \forall j \in J, \forall s \in S \quad (16)$$

$$\mathbb{C}_2 : \sum_{j=1}^{J} \max_{k \in B} \; Q_{i,s,j,k} \leq M \quad \forall i \in I, \forall s \in S \quad (17)$$

$$\mathbb{C}_3 : \sum_{s=1}^{S} \max_{j \in L} \max_{k \in B} \; Q_{i,s,j,k} \leq Z \quad \forall i \in I \quad (18)$$

The constraint C_1 ensures that each RB_k can only be assigned to a single UT_i. On the other hand, C_2 restricts a UT_i to not having more than *M CCs*, constraint C_3 allows for MC with up-to *Z* different satellites of similar or different orbits.

2) Constraint on Transmit Data Rate: The transmit data rate must be above a set threshold, hence C_4 guarantees the UT_i operates above minimum data rate.

$$\mathbb{C}_4 : R_i = \sum_{s=1}^{S} \sum_{j=1}^{J} \sum_{k=1}^{K} Q_{i,s,j,k}.R_{i,s,j,k} \geq R_i^{min} \; \forall i \in N \quad (19)$$

3) Constraint on Transmit Power: The UT_i transmit power should not exceed the maximum transmit power required of the link as in constraint C_5.

$$\mathbb{C}_5 : P_i = \sum_{s=1}^{S} \sum_{j=1}^{J} \sum_{k=1}^{K} Q_{i,s,j,k}.P_{i,s,j,k} \leq P_i^{max} \; \forall i \in N \quad (20)$$

4) Constraint on Delay: Constraint C_6 ensures that the UE_i operates below maximum latency.

$$\mathbb{C}_6 : D_i = max\{Q_{i,s,j,k}.D_{i,j,k}\} \leq D_i^{max} \; \forall i \in N \quad (21)$$

5) Constraint on QoS Threshold: In C_7 the orbital link QoS must be above the threshold in order to be utilized.

$$\mathbb{C}_7 : min\left\{ \frac{E_b}{N_o}_L, \frac{E_b}{N_o}_M, \frac{E_b}{N_o}_G \right\} > \eta \; \forall, s, j, k, \; and \; \forall i \quad (22)$$

IV. Optimization Problem Solutions

The energy efficient maximization and capacity enhancement problem with the objective function in (13) and constraints C_1 to C_7 outlined above is a non-convex optimization problem; these constraints comprise of inequality constraints. This problem is combinatorial because it is intended to search and arrive at a combination of variables (which includes RBs, CCs and satellites) from many different available options under the mentioned constraints which optimizes an index (E_η). It is non-convex due to the maximization of the objective function, and similarly constraint C_4 is non-convex. The combinatorial optimization problem in (13) with constraints C_1 to C_7 is difficult to solve. For the sake of tractability, two approaches are used to solve this problem; first approach is by decoupling the problem into two optimization sub-problems, while the second option is a heuristic approach.

A. Sub-Problem Decoupling Approach

This approach involves subdividing the problem into the joint route and power allocation sub-problem and the path matching sub-problem.

1) Joint Route and Power Allocation: The joint route and power allocation sub-problem is represented as (23).

$$\eta = \max_{Q_{i,s,j,k}, P_i} \sum_{i=1}^{I} \sum_{s=1}^{S} \sum_{j=1}^{J} \sum_{k=1}^{K} E_{\eta i}.Q_{i,s,j,k} \quad (23)$$

subject to $C_1 - C_5$.

This problem is solved using the interior point algorithm (IPA) which offers a fast convergence in solving nonlinear programming problems especially the large scale ones [42].

a) Interior point algorithm: In this subsection, attempt is made to solve the sub-problem of (23) by using IPA which can serve as a linear and nonlinear programming solver [43]. This work uses the IPA from [44], adapted to the problem at hand.

IPA finds the minimum value of a convex objective function. The objective function in this case is non-convex which can be converted to convex by negating the function, and the inequality constraints $C_1 - C_5$ are considered. The corresponding problem for IPA is represented as a general nonlinear program model in (24), for ease of comprehension and presentation, the problem in (23) is adapted into it with further IPA solutions to follow.

$$\begin{aligned} &\min_{p} \; -f(p) \\ &\text{subject to} \; \; g(p) \leq 0 \end{aligned} \quad (24)$$

The approximate minimization problem in (24) with the interior-point algorithm is difficult to solve because of the inequality constraints, hence this will be simplified having $\xi > 0$ as,

$$\min_{p,v} f_\xi(p, v) = \min_{p,v} f(p) - \xi \sum_i \ln(v_i) \quad (25)$$

subject to

$$v \geq 0, g(p) + v = 0.$$

The $v = \{v_1, v_2, v_3, \ldots\}$ represents the slack variables that are many as the inequality constraints *g*. The *v* variables are made positive to maintain the iterates in the interior of the feasible region. Hence when ξ (which is the barrier parameter) moves towards zero, the minimum of f_ξ extends to the minimum of *f*, while the logarithmic inserted in (25) represents a barrier function [45]. The transformation for the inequality constraint is applied to the constraints in (23), resulting in the new constraints outlined below.

$$\mathbb{C}_{1a} : \sum_{i=1}^{I} Q_{i,s,j,k} - 1 + v_1 = 0 \; \forall k \in K, \forall j \in J, \forall s \in S$$

$$\mathbb{C}_{2a} : \sum_{j=1}^{J} \max_{k \in B} \; Q_{i,s,j,k} - M + v_2 = 0 \; \forall i \in I, \forall s \in S$$

$$\mathbb{C}_{3a}: \sum_{s=1}^{S} \max_{j\in L} \max_{k\in B} Q_{i,s,j,k} - Z + v_3 = 0 \ \forall i \in I$$

$$\mathbb{C}_{4a}: \sum_{s=1}^{S}\sum_{j=1}^{J}\sum_{k=1}^{K} Q_{i,s,j,k}.R_{i,s,j,k} - R_i^{min} + v_4 = 0 \ \forall i \in N$$

$$\mathbb{C}_{5}a: \sum_{s=1}^{S}\sum_{j=1}^{J}\sum_{k=1}^{K} Q_{i,s,j,k}.P_{i,s,j,k} - P_i^{max} + v_5 = 0 \ \forall i \in N$$

The solution from (25) is obtained by using the Newton step in (p, v) at each iteration. The step tries to solve the Karush–Kuhn–Tucker (KKT) conditions in (26) and (27) through a linear approximation, the KKT equations give necessary and sufficient conditions for solving the minimization problem [46].

$$\nabla_p L(p, v, \lambda) = 0 \tag{26}$$

$$\lambda_g g_i(p) = 0 \ \forall_i \tag{27}$$

These KKT conditions use the Lagrangian function of

$$L(p, v, \lambda) = f_\xi(p, v) + \sum \lambda_g g_i(p) \tag{28}$$

where λ_g is the Lagrange multipliers. For each iteration, the algorithm attempts to decrease a merit function as

$$f_\xi(p, v) + \varsigma \|g(p) + v)\| \tag{29}$$

The parameter ς might increase with the iteration number so as to force the solution to a feasible point. This Newton step also known as the direct step uses the Hessian (H) of the Lagrangian of f_ξ as

$$H = \nabla^2 f_\xi(p) + \sum_i \lambda_i \nabla^2 g_i(p) \tag{30}$$

The outcome of attempting to solve for the KKT conditions using the linearized Lagrangian yields this matrix equation

$$\begin{bmatrix} H & 0 & 0 & J_g \\ 0 & \Lambda & 0 & V \\ J_g & I & 0 & 0 \end{bmatrix} \begin{bmatrix} \nabla_p \\ \nabla_v \\ \nabla_\lambda \end{bmatrix} = - \begin{bmatrix} \nabla_f + J_g\lambda \\ V\lambda - \xi e \\ g + v \end{bmatrix} \tag{31}$$

where J is the Jacobian of the respective constraint functions, λ is the Lagrange multiplier vector for inequality constraint g, e is the vector of ones with the same size as g, V is diag(v) and Λ is the diag(λ) [47], [48]. To solve for (∇_p, ∇_v), LDL factorization of the matrix is performed. LDL factorization allows for the unique factorization of the square Hermitian positive definite input of matrix $W = LDL^+$, where L is lower triangular matrix with elements that are unity diagonal, L^+ is the complex conjugate transpose of L; the diagonal matrix is represented as D [49].

As mentioned earlier, we utilize the available IPA solvers adapted to our problem. In particular, we are faced with the binary nature of the entries of Q. To incorporate the binary optimization under IPA, we relax Q to take values in the interval [0, 1] and use the entropy penalty function

$$\mathbb{F}(Q) = C_t * (-Q\log_2(Q) + ((1-Q)\log_2(1-Q))) \tag{32}$$

to the objective function, where C_t is a defined constant, to impose binary restrictions

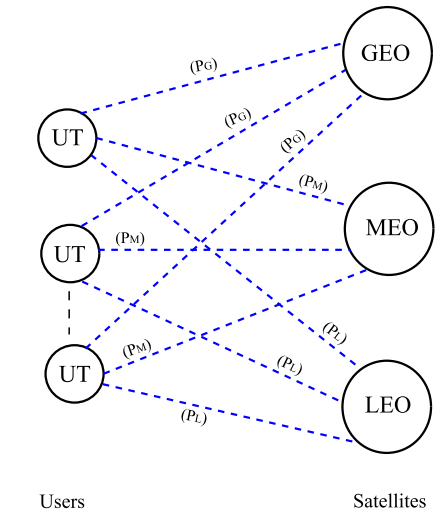

(a) Initial route selection and power allocation.

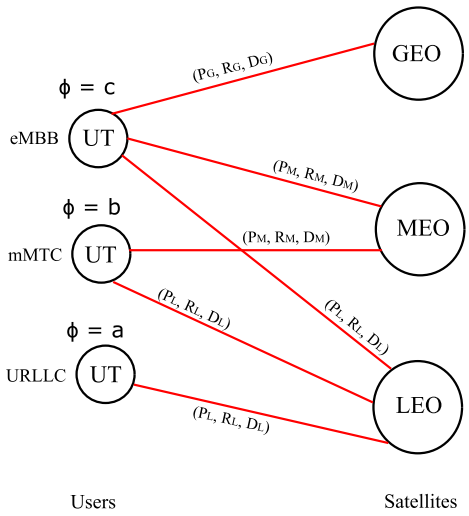

(b) Path matching.

Fig. 5. Route selection and path matching.

The optimization problem in (24) is solved with the IPA by obtaining P_i for (23) as illustrated in Fig. 5a. With this, the joint route and power allocation sub-problem is solved; it paves the way for the path matching sub-problem to be solved.

2) Path Matching Sub-Problem: The path matching sub-problem is expressed in (33) with the addition of constraints C_8, C_9 and C_{10}. The $\phi = \{a, b, c, 0\}$ is a set of service classes where a, b, c stands for URLLC, mMTC and eMBB services, respectively. 0 is included to account for PDUs that may not be identifiable into any of the three service classes defined. The aim is to solve for the perfect path match (Q^*) that ensures EE is maximized.

$$\max_{Q^*_{i,s,j,k}} \ \phi_i \eta_i \tag{33}$$

subject to $C_6 - C_{10}$

$$C_8: R_i^* = \begin{cases} R_{iL} & \text{if } \phi = a \\ R_{iM} + RiL & \text{if } \phi = b \\ R_{iG} + R_{iM} + R_{iL} & \text{if } \phi = c \\ 0 & \text{otherwise} \end{cases} \tag{34}$$

Algorithm 1: Service Classification and Segmentation

Input: P_s = Arriving terminal PDUs
ID_s = Service ID
σ = Total number of transmitted PDUs
$j = 1$
Output: Q^a, Q^b, and Q^c

while $j \leq \sigma$ **do**
  if $\phi_k^i = a$ **then**
    Classify and Segment P_s as URLLC
  end
  if $\phi_k^i = b$ **then**
    Classify and Segment P_s as mMTC
  end
  if $\phi_k^i = c$ **then**
    Classify and Segment P_s as eMBB
  end
  if $\phi_k^i = 0$ **then**
    Return to step 2
  end
end

$$C_9 : P_i^* = \begin{cases} \max(P_{iL}) & \text{if } \phi = a \\ \max(P_{iM}, P_{iL}) & \text{if } \phi = b \\ \max(P_{iG}, P_{iM}, P_{iL}) & \text{if } \phi = c \\ 0 & otherwise \end{cases} \quad (35)$$

$$C_{10} : D_i^* = \begin{cases} \max(D_{iL}) & \text{if } \phi = a \\ \max(D_{iM}, D_{iL}) & \text{if } \phi = b \\ \max(D_{iG}, D_{iM}, D_{iL}) & \text{if } \phi = c \\ 0 & otherwise \end{cases} \quad (36)$$

The constraints C_8 indicates the optimal data rate for the different service class, while C_9 and C_{10} represents the optimum transmit power and delay based on the service class in question. Since the route selection and power allocation strategy have both been solved, solution can now be derived for the path matching strategy. The UT path matching sub-problem is solved by modelling the uplink transmission network, as a weighted bipartite graph. The system is modelled as a weighted bipartite graph $G' = \{U', E', W'\}$, where U' represents the set of UTs, $E' = \{E'_{U,S}\}$ denotes the set of paths between the UTs and the satellites S'; $W' = \{_{\eta_i, P_i}\}$ is the weight sets (comprising of power, data rate and delay) between links E'.

A path weighted matching technique (PWMT) is used to arrive at the optimal path matching strategy that offers the maximum energy efficiency while satisfying the service class requirements. The PWMT was used in a seemingly small scale, however in a larger scale involving many UTs and satellites, the Hungarian algorithm can be applied which is presented from literature for completeness in the Appendix-A. At this stage, PWMT is applied to solve the sub-problem as illustrated in Fig. 5(b). Hence the optimal solution of the problem is obtained.

B. Proposed Algorithm

The proposed algorithm is known as the EE-SAMC algorithm, which uses the service aware multi-layer NTN resource scheduling architecture shown in Fig. 3. The resource scheduling process commences with control plane signaling, where the service classification and segmentation of the UTs is performed using the SSU in the RLC sublayer, which segments the UTs to different queues of URLLC (a), mMTC (b) and eMBB (c) with Algorithm 1, also using the SID of the UTs as a differentiating identifier. Once the UT service class is known, the respective UTs are scheduled to appropriate resources including RBs, CCs and satellites that satisfy the QoS requirement of the service class in question, this scheduling is achieved using the EE-SAMC scheduling-Algorithm 2 at the RS unit in the MAC sublayer of the HGS. As the UTs transmit the PDUs in the user plane to the RAN, the PDUs arrive with arrival rate A to the appropriate RAN resources as described in Section II-A.

The EE-SAMC algorithm defines the number of users, RBs, CCs and satellites; it considers the following parameters, the $\frac{E_b}{N_o}$ of the orbital satellites and the queue length of the respective service classes from Algorithm 1. It then solve for the route selection and power allocation strategy using (23); then the path matching strategy is obtained by solving (33) with the PWMT in Section IV-A2. EE-SAMC algorithm then begins to perform the decision phase, by confirming if the $\frac{E_b}{N_o}$ values of the orbital satellites in view satisfy the QoS

Algorithm 2: Energy Efficient Service Aware Multi-Connectivity Scheduler

Number of users = I; Number of CCs = J; Number of RBs = K; Number of satellites = S.
Input: $\frac{E_b}{N_o} L$ = *QoS for LEO*, $\frac{E_b}{N_o} M$ = *QoS for MEO*, $\frac{E_b}{N_o} G$ = *QoS for GEO*
Q^a = Length of URLLC PDUs
Q^b = Length of mMTC PDUs
Q^c = Length of eMBB PDUs
$\sigma = Q^a + Q^b + Q^c$, $\eta = E_b/N_o$ Threshold,
$t = 1$
Route Selection and Power allocation strategy
Solve the problem in (23) with IPA to obtain P_i
Multi-connectivity strategy
Implement while considering C_7 (22)
while $t \leq \sigma$ **do**
  if E_b/N_{oG} *and* E_b/N_{oM} *and* $E_b/N_{oL} > \eta$ **then**
    Implement MC using all orbital carriers
  end
  if E_b/N_{oG} *and* $E_b/N_{oM} > \eta$ **then**
    Implement DC using GEO and MEO CCs
  end
  if E_b/N_{oG} *and* $E_b/N_{oL} > \eta$ **then**
    Implement DC using GEO and LEO CCs
  end
  if E_b/N_{oM} *and* $E_b/N_{oL} > \eta$ **then**
    Implement DC using LEO and MEO CCs
  end
  revert to single carrier mode on any available carrier
end
Path matching strategy
Solve the path matching sub-problem in (33) to obtain Q^*
Optimum solution obtained for (15):
$\max_{Q_{i,s,j,k}, P_i} \sum_{i=1}^{I} \sum_{s=1}^{S} \sum_{j=1}^{J} \sum_{k=1}^{K} \phi_i^* E\eta_i . Q_{i,s,j,k}$
with C_1 *to* C_7

TABLE II
LINK PARAMETERS SPECIFIED BY 3GPP RELEASE 16 [50] AND ANALYTICALLY DERIVED

Parameters	LEO S-band	LEO Ka-band	MEO S-band	MEO Ka-band	GEO S-band	GEO Ka-band
Orbit altitude (Km)	1,200 ✓	1,200 ✓	10,000 ✓	10,000 ✓	35,786 ✓	35,786 ✓
Propagation range (Km)	2,942 †	2,942 †	10,752 †	10,752 †	36,343 †	36,343 †
UT elevation angle (degrees)	12.43 †	12.43 †	54.70 †	54.70 †	63.88 †	63.88 †
Satellite G/T (dB/K)	1.1 ✓	13 ✓	10 *	20 *	19 ✓	28 ✓
UL carrier frequency (GHz)	2 ✓	30 ✓	2 *	30 *	2 ✓	30 ✓
Bandwidth (MHz)	20 ✓	100 ✓	20 *	100 *	20 ✓	100 ✓
UT circuit consumption (dBm)	23 *	26.98 *	23 *	26.98 *	23 *	26.98 *
UT Tx gain (dBi)	0 ✓	43.20 ✓	0 *	43.20 *	0 ✓	43.20 ✓
UT transmit power (dBm)	49 †	29.03 †	51 †	29.54 †	53 †	30 †
Free space loss (dB)	167.84 †	191.36 †	179.09 †	202.62 †	189.67 †	213.19 †
Received isotropic power (dBW)	-156.63 †	-156.35 †	-165.60 †	-167.38 †	-174.18 †	-177.51 †
Uplink C/N (dB)	-0.16 †	4.47 †	-0.51 †	0.72 †	-0.09 †	-1.41 †
Eb/No (dB)	2.84 †	14.47 †	2.49 †	10.72 †	2.91 †	8.59 †
Data rate (Mbps)	24.00 †	133.55 †	24.49 †	131.07 †	26.10 †	130.68 †
Modulation	QPSK ‡	16QAM ‡	QPSK ‡	8PSK ‡	QPSK ‡	8PSK ‡
Code rate	1/3 ‡	5/6 ‡	1/3 ‡	5/6 ‡	1/3 ‡	3/4 ‡
✓ 3GPP, † Analytically derived, * Assumed, ‡ DVB-RCS2						

threshold requirement. If $\frac{E_b}{N_o}_L$, $\frac{E_b}{N_o}_M$ and $\frac{E_b}{N_o}_G$ satisfy the QoS threshold, then MC is performed. But if only two of any of the orbital links meets the threshold, then DC is performed with the satisfying links, else the algorithm reverts to single carrier mode to provision and maintain the network connectivity.

C. Heuristic Approach

This approach heuristically derives a weighting factor α to arrive at an energy efficient with uplink MC resource allocation pattern for the UTs on different orbital satellite links of LEO, MEO and GEO, while considering the service class of URLLC, mMTC and eMBB ascribed to the UTs. A link budget analysis is performed as shown in Table II, where the $\frac{C}{N}$ values of the orbital links are obtained from Table II. The obtained $\frac{C}{N}$ values is applied into (37) - (41), to derived the corresponding weighting factor α. Then ultimately the α_L, α_M and α_G values are obtained using (42) - (44), which defines the allocation pattern.

D. Bench-Mark Approach

Two other bench-marking approaches are described below which are used in Section V-D, for comparison with the performance of the proposed optimization algorithm and the Heuristic approach.

1) Random Allocation Scheduling Approach: This random allocation (RA) scheduling approach uses the different orbital transmission power of LEO, MEO and GEO as shown in Table II, and the allocation pattern is derived in a random distribution, without any preferential consideration given to neither the orbital resource nor the UT service class. This approach is considered due to its low-complexity and fast allocation capability.

$$\alpha''^{a}_{L} = \frac{\frac{\frac{C}{N}^{a}_{L}}{\frac{C}{N}^{a}_{L}+\frac{C}{N}^{a}_{M}+\frac{C}{N}^{a}_{G}}}{\left(\frac{\frac{C}{N}^{a}_{L}}{\frac{C}{N}^{a}_{L}+\frac{C}{N}^{a}_{M}+\frac{C}{N}^{a}_{G}}\right)+\left(\frac{\frac{C}{N}^{b}_{L}}{\frac{C}{N}^{b}_{L}+\frac{C}{N}^{b}_{M}+\frac{C}{N}^{b}_{G}}\right)+\left(\frac{\frac{C}{N}^{c}_{L}}{\frac{C}{N}^{c}_{L}+\frac{C}{N}^{c}_{M}+\frac{C}{N}^{c}_{G}}\right)} \tag{37}$$

$$\alpha''^{b}_{L} = \frac{\frac{\frac{C}{N}^{b}_{L}}{\frac{C}{N}^{b}_{L}+\frac{C}{N}^{b}_{M}+\frac{C}{N}^{b}_{G}}}{\left(\frac{\frac{C}{N}^{a}_{L}}{\frac{C}{N}^{a}_{L}+\frac{C}{N}^{a}_{M}+\frac{C}{N}^{a}_{G}}\right)+\left(\frac{\frac{C}{N}^{b}_{L}}{\frac{C}{N}^{b}_{L}+\frac{C}{N}^{b}_{M}+\frac{C}{N}^{b}_{G}}\right)+\left(\frac{\frac{C}{N}^{c}_{L}}{\frac{C}{N}^{c}_{L}+\frac{C}{N}^{c}_{M}+\frac{C}{N}^{c}_{G}}\right)} \tag{38}$$

$$\alpha''^{c}_{L} = \frac{\frac{\frac{C}{N}^{c}_{L}}{\frac{C}{N}^{c}_{L}+\frac{C}{N}^{c}_{M}+\frac{C}{N}^{c}_{G}}}{\left(\frac{\frac{C}{N}^{a}_{L}}{\frac{C}{N}^{a}_{L}+\frac{C}{N}^{a}_{M}+\frac{C}{N}^{a}_{G}}\right)+\left(\frac{\frac{C}{N}^{b}_{L}}{\frac{C}{N}^{b}_{L}+\frac{C}{N}^{b}_{M}+\frac{C}{N}^{b}_{G}}\right)+\left(\frac{\frac{C}{N}^{c}_{L}}{\frac{C}{N}^{c}_{L}+\frac{C}{N}^{c}_{M}+\frac{C}{N}^{c}_{G}}\right)} \tag{39}$$

$$\alpha'^{a}_{L} = \frac{\alpha''^{a}_{L}}{\alpha''^{a}_{L}+\alpha''^{a}_{M}+\alpha''^{a}_{G}+\alpha''^{b}_{L}+\alpha''^{b}_{M}+\alpha''^{b}_{G}+\alpha''^{c}_{L}+\alpha''^{c}_{M}+\alpha''^{c}_{G}} \tag{40}$$

$$\alpha^{a}_{L} = \frac{\left(\frac{\alpha'^{a}_{L}}{\alpha'^{a}_{L}+\alpha'^{a}_{M}+\alpha'^{a}_{G}}\right)}{N_c} \tag{41}$$

$$\alpha_L = \left\{\alpha^{a}_{L}, \alpha^{b}_{L}, \alpha^{c}_{L}\right\} \tag{42}$$

$$\alpha_M = \left\{\alpha^{a}_{M}, \alpha^{b}_{M}, \alpha^{c}_{M}\right\} \tag{43}$$

$$\alpha_G = \left\{\alpha^{a}_{G}, \alpha^{b}_{G}, \alpha^{c}_{G}\right\} \tag{44}$$

It should be noted that $0 \leq \alpha^{i}_{k} \leq 1$, where i represents the service class of URLLC (a), mMTC (b) or eMBB (c); k represents orbital satellite links of LEO (L), MEO (M) or GEO (G); N_c represents the number of service classes. The same notation applies to $\frac{C}{N}^{i}_{k}$.

2) Round Robin Scheduling Approach: This scheduling approach makes use of the orbital transmission power of LEO, MEO and GEO as shown in Table II. The resource allocation pattern is obtain using the round robin (RR) mechanism in [10], which allocates resources in a cyclic proportional pattern across all CCs regardless of all channel constraints.

V. PERFORMANCE EVALUATION

In this section, the simulation configurations are outlined, along with discussions on the performance analysis of the proposed algorithm.

A. Simulation Setup

The simulation was setup to solve the problems and sub-problems mentioned in Section IV-A. In addition,

more simulations were setup with a link budget analysis using parameters outlined in Table II for the Heuristic approach scheduler. MATLAB was also used to simulate the performance of the proposed algorithm in terms of energy efficiency, throughput and delay while comparing other state-of-the-art algorithms. It is important to note that the link budget parameters used for analysis is the one related to Ka-band for LEO, MEO and GEO. This is because Ka-band UT uses a lower transmit power compared to the S-band UT which has a lower gain of 0 dBi resulting to a lower EIRP compared to the Ka-band; similarly the s-band satellites have lower G/T values compared to Ka-band satellites. In addition, s-band is a frequency range that is used for 4G and 5G NR [51], [52], and it has a limited bandwidth up to 30 MHz, while Ka-band offers a higher bandwidth of up to 400 MHz [50], and 100MHz with 20MHz have been adopted for Ka-band and S-band respectively in this paper; even if three CCs of LEO, MEO and GEO are aggregated with 20MHz each it will result to only 60MHz which is less than 100 MHz (for a single CC) from Ka-band. A uniform band is also used across the three orbits, in order to minimize the complexity at the UT. The modulation and code rate (MODCOD) scheme impact is captured in the different Eb/No and C/N values of the link budget for the three orbital links, which demonstrates the performance of the air interface to limit the impact of the satellite channel noise and ensure the condition in constraint C_7 is satisfied with acceptable QoS value above the threshold set. The MODCOD is adopted of DVB-RCS2 air interface parameters, by mapping the resultant E_b/N_o of the link budget analysis to related ones as specified in [53].

B. Concept Evaluation of Multi-Connectivity

In this subsection, the advantages of using MC over single connectivity is discussed. Here we have three orbital satellite constellation resources with three service class demands, the constraints on the service class requirement is summarised in Section II-B. The available satellite resources include LEO, MEO and GEO orbital satellites with different characteristics some of which are mentioned in Table II. These resources are in form of frequency blocks called component carriers (CCs), that are made up of a collection of resource blocks (RBs), these RBs are time-frequency resources over which transmissions are scheduled. Hence packets can be scheduled for transmission over the satellites of the three orbits simultaneously, the transmitted information is multiplexed and not duplicated.

The achievable data rate (uplink capacity) enhancement which is an added feature is a non-convex linear optimization problem, and this problem can be solved by the aggregation of the allocated capacity of the CCs of the orbital satellites LEO, MEO and GEO, which can enable the realisation of the data rate requirement of use-case services especially eMBB. Using the parameters in Table II data rate and EE with respect to traffic load is shown in Fig. 6. Precisely Fig. 6a shows that with DC and MC higher peak data rate can be achieved by using (12) compared to single carrier connectivity (SC) links. DC of LEO/MEO and LEO/GEO performs

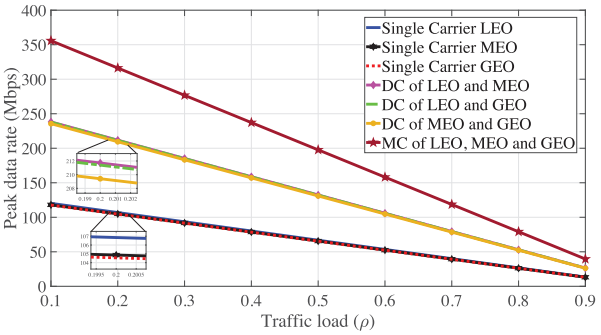

(a) Peak data rate with respect to traffic load.

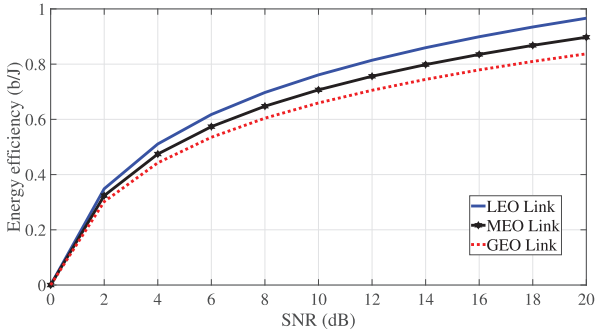

(b) Normalized orbital energy efficiency with respect to SNR.

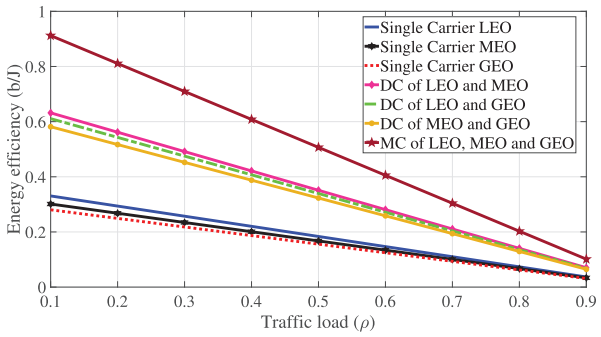

(c) Normalized energy efficiency with respect to traffic load.

Fig. 6. Evaluation of MC, DC and single carrier performance.

slightly better in peak data rate than DC of MEO/GEO due to the reduced FSL in the LEO CC which is a function of the satellite altitude; while MC of LEO/MEO/GEO out performs all carriers in data rate because of the aggregation of the three orbital CCs. It is also seen that DC and MC links maintain higher data rates trends over SC even as the traffic load increases. Another observation is the peak data rate performance trend of SC LEO, MEO and GEO which overlap, mainly because of the parameter variation described in Table II involving satellite Gain to temperature ratio (G/T), transmit power and resultant FSL. Which shows LEO to operate with a lowest transmit power (29.03 dBm), lowest satellite G/T (13 dBi) and FSL (191.36 dB); MEO operating with a transmit power of 29.54 dBm, satellite G/T of 20 dBi and FSL of 202.62 dB, while that of GEO is 30 dBm for transmit power, 28 dBi for satellite G/T and 213.19 dB for FSL. Hence these parameter values leads to the overlapping in peak data rate trends for the SC and DC trends.

It is important to note that the transmit power requirement for LEO, MEO and GEO CCs are different which is obvious in the energy efficiency in Fig. 6b, LEO has the highest energy efficiency because of the limited power required to satisfy the link budget due to the low altitude and low FSL. This also corresponds to the energy efficiency of the DC and MC links in Fig. 6c, where all SC perform below the DC and MC combinations. Consequently, MC out performs DC in EE, because of the higher achievable data rate transmission capable with MC, as seen in Fig. 6a. Furthermore, the EE performance of SC LEO is better than SC MEO and GEO because of the lower transmit power required in LEO, and also MEO when comparing to GEO. Similarly, DC LEO/MEO is better than DC LEO/GEO and DC MEO/GEO because of the lower transmit power required for LEO and MEO compared to the other two DC options. MC of LEO/MEO/GEO achieves higher energy efficiency and data rate than all other single and DC carriers. Multi-orbital MC is advantageous because it introduces robustness to the network which allows for resiliency and higher system capacity.

C. Algorithm Complexity Analysis

The total complexity cost involved in solving the problem using Algorithm 2, depends on the sum of cost of the IPA and PWMT together. The cost of using IPA to solve the joint route and power allocation sub-problem is a product of the number of iterations, including the computation required to determine the Newton direction in each iteration. The Newton direction can be determined by solving linear equations in (31). Recall that the general complexity involved in solving n linear equations with n unknowns is $O(n^3)$, however the cost of computation of the Newton step based on (31) is $O(n)$. If the log barrier function in (25) is a self-concordant function, the number of Newton iterations is considered polynomial and it depends on the structure of the function. The complexity of IPA translates to $O(\sqrt{n}\ log\frac{n}{\epsilon})$ Newton iterations required to arrive at a feasible and optimal solution, with error tolerance of ϵ, where n is the variables, which in our case is the sum of the number of UTs, RBs, CCs and satellites defined. As n increases, the execution time and complexity of the IPA increases. Hence, the complexity of IPA used in solving the joint route and power allocation sub-problem is $O(n^{1.5})$ [54], [55]. From the analysis of the simulation run time, the run time for network configuration comprising 3 variable counts for each of UTs, RBs, CCs and satellites is 0.024ms, while that with a configuration of 9 variable counts for each of UTs, RBs, CCs and satellites is 0.041ms.

The PWMT (Hungarian) algorithm increases complexity based on the increase in the number of user U' vertices in the bipartite graph, as $O(U'^3)$ [56].

D. Performance Analysis

The objective is to maximize the uplink energy efficiency of the UTs, whilst enhancing the data rate by implementing the MC technique using the EE-SAMC scheduler taking into consideration the requirements of the PDU service classifications. This is done by defining an optimal transmit power P and resource allocation pattern Q.

Likewise, the SAMC Heuristic scheduler also operates to maximize the uplink energy efficiency of the UTs, whilst enhancing the data rate by implementing the MC technique while taking into consideration the requirements of the UT service classifications. It achieves this by defining the transmit power from the link budget analysis in Table II, and then it generates the resource allocation pattern α as explained in Section IV-C. Both EE-SAMC and SAMC Heuristic schedulers do not allocate resources on MEO and GEO CCs for URLLC class of PDUs. Similarly, both only utilize LEO and MEO CCs when allocating PDUs for mMTC class of services; for eMBB class of services all three LEO, MEO and GEO CCs are used for PDU allocation.

The other two schedulers used as benchmark in this paper, are the RA and the RR schedulers. Both of them function by using the transmit power outlined in Table II from link budget analysis, but defined different allocation patterns. The Allocation pattern of RA is generated randomly using MATLAB program for each of the available orbital CCs without considering the service classifications. Similarly, RR also allocates PDUs on all available orbital CCs, in an equally proportionate manner without considering the service classifications.

In Fig. 7a, the data rate performance of the EE-SAMC scheduler is compared to heuristic, RR and RA schedulers, the data rate is plotted against maximum power (P Max). The achievable data rate R is derived using (12) with equal BW of 100 MHz set for each of the three orbital CCs. The plot shows that EE-SAMC achieves average data rate of 393.72 Mbps at P Max of 1 dBW, the Heuristic scheduler also achieves 390.14 Mbps data rate while RR and RA performed at 381.02 Mbps and 374.82 Mbps respectively when P Max is 1 dBW. This shows that EE-SAMC out performs the Heuristic, RR and RA by 0.91%, 3.27% and 4.91% respectively. Further observation of the same chart trend shows that EE-SAMC out performs other schedulers.

In Fig. 7b, the energy efficiency in b/J is plotted against P Max in dBW, and it shows the EE performance of EE-SAMC compared with the Heuristic, RR and RA schedulers. When P Max is 1 dBW, EE-SAMC attains energy efficiency of 0.83 b/J, while Heuristic, RR and RA schedulers perform at 0.82 b/J, 0.80 b/J and 0.78 b/J respectively. This shows that EE-SAMC out performs the Heuristic, RR and RA by 1.21%, 3.68% and 6.21% respectively.

Similarly in Fig. 8a, where energy efficiency is plotted against signal-to-noise ratio (SNR) in dB. The energy efficiency performance shows that EE-SAMC achieved 0.80 b/J at 12 dB, while the Heuristic, RR and RA schedulers achieve 0.77 b/J, 0.75 b/J and 0.74 b/J respectively. It further shows that EE-SAMC out performs the Heuristic, RR and RA by 3.82%, 6.45% and 7.79% respectively.

Furthermore, performance evaluation is done using Fig. 8b of energy efficiency against bandwidth in MHz. It shows that EE-SAMC achieves EE of 0.75 b/J at BW of 120 MHz, while the Heuristic, RR and RA schedulers achieve 0.72 b/J, 0.70 b/J and 0.69 b/J respectively. This shows that EE-SAMC

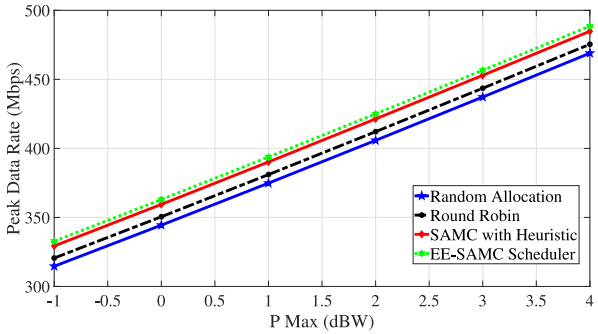

(a) Peak data rate with respect to P Max.

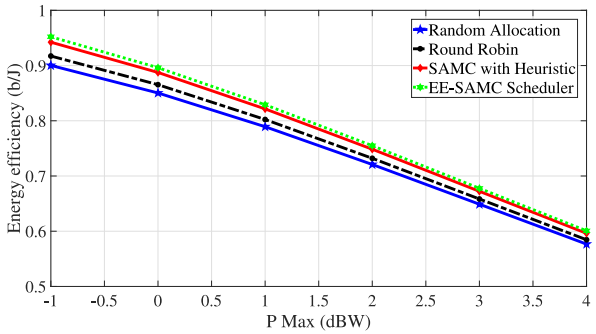

(b) Normalized energy efficiency with respect to P Max.

Fig. 7. Evaluation of PMax in peak data rate and energy efficiency.

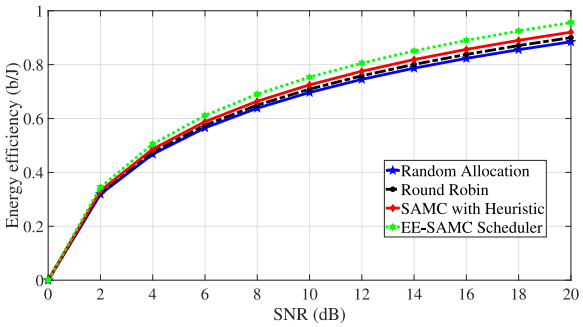

(a) Normalized energy efficiency with respect to SNR.

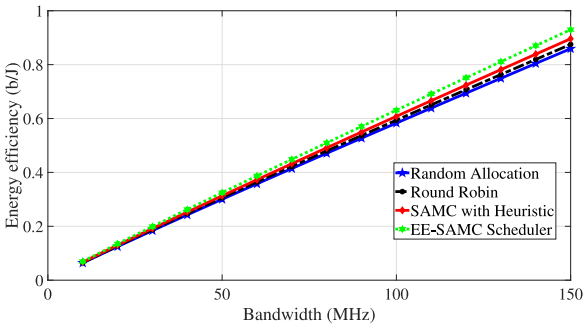

(b) Normalized energy efficiency with respect to Bandwidth.

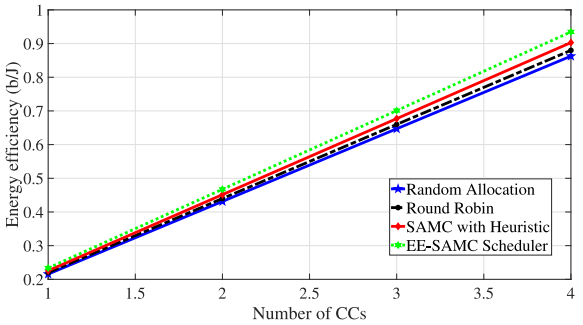

(c) Normalized energy efficiency with respect to CCs.

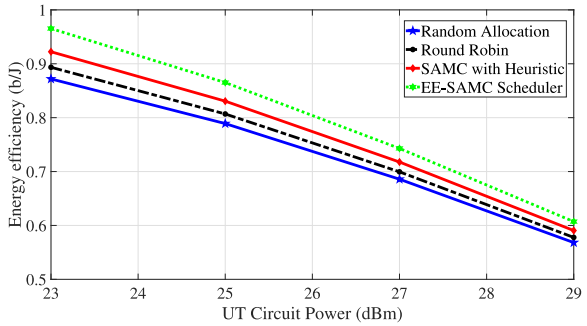

(d) Normalized energy efficiency with respect to UT circuit power

Fig. 8. Evaluation of normalized energy efficiency with SNR, bandwidth, CCs and UT circuit power.

out performs the Heuristic, RR and RA by 4.08%, 6.89% and 8.33% respectively. In Fig. 8c, the performance of energy efficiency verse number of CCs is shown for EE-SAMC scheduler compared to Heuristic, RR and RA schedulers. The plot shows that at 4 CCs, EE-SAMC achieves 0.93 b/J, while the Heuristic, RR and RA schedulers achieve 0.90 b/J, 0.87 b/J and 0.86 b/J respectively. Which shows that EE-SAMC out performs the Heuristic, RR and RA by 3.27%, 6.66% and 7.82% respectively.

The performance evaluation of EE verse UT circuit power (P_c) is shown in Fig. 8d. It shows that EE-SAMC achieves EE of 0.74 b/J at P_c of 27 dBm, while the Heuristic, RR and RA schedulers achieve 0.71 b/J, 0.69 b/J and 0.68 b/J respectively. This shows that EE-SAMC out performs the Heuristic, RR and RA by 4.13%, 6.99% and 8.45% respectively.

Finally, in Fig. 9 the performance of delay in ms of URLLC class of services are evaluated against number of CCs. The

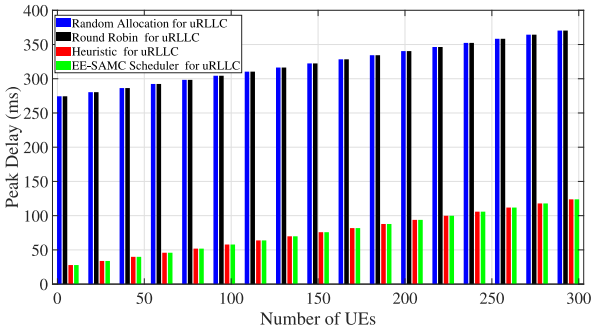

Fig. 9. Peak delay with respect to number of UTs for URLLC service class.

delay performance shows that EE-SAMC achieved 93.83 ms when number of users is 200, while the Heuristic, RR and RA schedulers achieved 93.83 ms, 340.37 ms and 340.37 ms respectively. This shows that EE-SAMC and the

Heuristic schedulers achieve similar delay performance with the heuristic scheduler because they consider the service class during scheduling, and the URLLC PDUs are only allocated to the LEO CC. The RR and RA both achieved the same delay performance and are higher than EE-SAMC and heuristic schedulers, this is so because the schedulers do not consider the service class when scheduling the PDUs, they utilize any of the three orbital CCs of LEO, MEO and GEO for all service classes using their respective allocation patterns. Hence both of EE-SAMC and Heuristic out performed the RR and RA schedulers by 113.56% and 113.56% respectively.

During the scheduling process it was discovered that RR and RA showed limitations on the ability to dimension resources whilst considering the requirements of the service class of URLLC, mMTC and eMBB. This further impacted their energy efficiency, data rate and URLLC delay performance. EE-SAMC slightly out performed the Heuristic schedulers due to the fact that EE-SAMC allocates power in a more efficient pattern compared to the latter, nonetheless both showed robustness without much limitations in resource allocation, as they can route traffic intelligently in an optimal pattern while considering the requirements of the service classes of URLLC, mMTC and eMBB, where energy efficiency, data rate and delay are optimized with efficient utilization of the spectrum and system power resources. This confirms EE-SAMC is a superior scheduler compared to the Heuristic, RR and RA schedulers.

VI. Conclusion

In this paper, a multi-layer NTN network topology is considered that connects to LEO, MEO and GEO satellites simultaneously, which uses a HGS that employs softwarized controllers, NFV elements and scheduling algorithms for the optimization of uplink energy efficiency, throughput, delay and guarantees resiliency. A service-aware multi-layer scheduling architecture is also crafted with adaptation into the protocol stack, which shows user and control plane implementation framework. Furthermore, the optimization of uplink energy efficiency, throughput and delay in a multi-layer satellite network is explored, by employing intelligent resource allocation strategies. Two approaches were analyzed involving optimization and heuristic algorithms, which were designed from combinatorial non-convex problem with linear inequality constraints and link budget analysis. These approaches took into account the service class of the transmitted PDUs and used MC to enhance throughput. From result analysis, our proposed scheduler (EE-SAMC) outperformed the heuristic and other state-of-the-art schedulers in terms of EE and throughput. A future research area could include exploiting the features of deep machine learning in solving the combinatorial optimization problem.

Appendix

A. The Hungarian Algorithm With Proof of Matching

This Appendix, from literature, is provided for completeness. The Hungarian algorithm is explained for large application of path matching and this approached is followed as in [57]. With a weighted bipartite graph of $G' = \{U', E', W'\}$, a feasible labeling (ℓ) is one that is

$$\ell(u') + \ell(s') \geq W'(u', s') \quad \forall u' \in U', \forall s' \in S' \tag{45}$$

The equality graph with respect to ℓ is $G' = (V, E'_\ell)$, where

$$E'_\ell = (u', s') : \ell(u') + \ell(s') = W'(u', s') \tag{46}$$

Theorem 1: If label (ℓ) is possible and M_p is a perfect matching in E_ℓ, it can then be said that M_p is a max-weight matching.

Proof: Defining edge $e \in E$ as $e = (e_u, e_s)$. Let M_p^* be any perfect matching in G. Since u $\in V$ is discovered exactly one time by M_p, it results that

$$w(M_p^*) = \sum_{e \in M_p^*} w(e) \leq \sum_{e \in M_p^*} (\ell(e_u) + (e_s)) = \sum_{v \in V} \ell(v) \tag{47}$$

Hence $\sum_{v \in V} \ell(v)$ is an upper-bound on the cost of any perfect matching. If M_p is the perfect matching in E_ℓ, then

$$w(M_p) = \sum_{e \in M_p} w(e) = \sum_{v \in V} \ell(v) \tag{48}$$

Therefore $w(M_p^*) \leq w(M_p)$ and M_p is optimal. ■

References

[1] M. N. Dazhi, H. Al-Hraishawi, B. Shankar, and S. Chatzinotas, "Terminal-aware multi-connectivity scheduler for uplink multi-layer non-terrestrial networks," in *Proc. IEEE Globecom Workshops*, Dec. 2022, pp. 1133–1139.

[2] M. Hosseinian, J. P. Choi, S.-H. Chang, and J. Lee, "Review of 5G NTN standards development and technical challenges for satellite integration with the 5G network," *IEEE Aerosp. Electron. Syst. Mag.*, vol. 36, no. 8, pp. 22–31, Aug. 2021.

[3] "Satellite earth stations and systems (SES); energy efficiency of satellite broadband network," ETSI, Sophia Antipolis, France, Rep. TR 103 352, Jun. 2016.

[4] Z. Zhang, W. Zhang, and F.-H. Tseng, "Satellite mobile edge computing: Improving QoS of high-speed satellite-terrestrial networks using edge computing techniques," *IEEE Netw.*, vol. 33, no. 1, pp. 70–76, Jan./Feb. 2019.

[5] F. Héliot and R. Tafazolli, "Optimal energy-efficient source and relay precoder design for two-way MIMO-AF relay systems," *IEEE Trans. Green Commun. Netw.*, vol. 4, no. 3, pp. 759–773, Sep. 2020.

[6] L. Bertaux et al., "Software defined networking and virtualization for broadband satellite networks," *IEEE Commun. Mag.*, vol. 53, no. 3, pp. 54–60, Mar. 2015.

[7] H. Al-Hraishawi, H. Chougrani, S. Kisseleff, E. Lagunas, and S. Chatzinotas, "A survey on nongeostationary satellite systems: The communication perspective," *IEEE Commun. Surveys Tuts.*, vol. 25, no. 1, pp. 101–132, 1st Quart., 2023.

[8] H. Al-Hraishawi, S. Chatzinotas, and B. Ottersten, "Broadband nongeostationary satellite communication systems: Research challenges and key opportunities," in *Proc. IEEE Int. Conf. Commun. Workshops (ICC Workshops)*, Jun. 2021, pp. 1–6.

[9] T. Colin, T. Delamotte, and A. Knopp, "Filter distortions in ultra high-throughput satellites: Models, parameters and multicarrier optimization," *IEEE Trans. Signal Process.*, vol. 70, pp. 292–306, 2022.

[10] M. N. Dazhi, H. Al-Hraishawi, M. R. B. Shankar, and S. Chatzinotas, "Uplink capacity optimization for high throughput satellites using SDN and multi-orbital dual connectivity," in *Proc. IEEE Int. Conf. Commun. Workshops (ICC Workshops)*, May 2022, pp. 544–549.

[11] "Study on small cell enhancements for E-UTRA and E-UTRAN: Higher layer aspects," 3GPP, Sophia Antipolis, France, Rep. TR 36.842, Feb. 2014.

[12] H. Al-Hraishawi, N. Maturo, E. Lagunas, and S. Chatzinotas, "Scheduling design and performance analysis of carrier aggregation in satellite communication systems," *IEEE Trans. Veh. Technol.*, vol. 70, no. 8, pp. 7845–7857, Aug. 2021.

[13] D. Wang, M. Giordani, M.-S. Alouini, and M. Zorzi, "The potential of multilayered hierarchical nonterrestrial networks for 6G: A comparative analysis among networking architectures," *IEEE Veh. Technol. Mag.*, vol. 16, no. 3, pp. 99–107, Sep. 2021.

[14] "Technical specification group radio access network; study on new radio (NR) to support non-terrestrial networks (release 15)," 3GPP, Sophia Antipolis, France, Rep. TR 38.811, Jun. 2019.

[15] *Evolved Universal Terrestrial Radio Access (E-UTRA) and NR; Multi-Connectivity; Stage 2*, 3GPP Standard TS 37.340, Sep. 2019.

[16] H. Cui et al., "Space–air–ground integrated network (SAGIN) for 6G: Requirements, architecture and challenges," *China Commun.*, vol. 19, no. 2, pp. 90–108, Feb. 2022.

[17] V. F. Monteiro, D. A. Sousa, T. F. Maciel, F. R. P. Cavalcanti, C. F. M. e. Silva, and E. B. Rodrigues, "Distributed RRM for 5G multi-RAT multiconnectivity networks," *IEEE Syst. J.*, vol. 13, no. 1, pp. 192–203, Mar. 2019.

[18] R. P. Antonioli, J. Pettersson, and T. F. Maciel, "Split responsibility scheduler for multi-connectivity in 5G cellular networks," *IEEE Netw.*, vol. 34, no. 6, pp. 212–219, Nov./Dec. 2020.

[19] H. Al-Hraishawi, E. Lagunas, and S. Chatzinotas, "Traffic simulator for multibeam satellite communication systems," in *Proc. 10th Adv. Satellite Multimedia Syst. Conf. 16th Signal Process. Space Commun. Workshop (ASMS/SPSC)*, Oct. 2020, pp. 1–8.

[20] A. Mahbas, H. Zhu, and J. Wang, "Trio-connectivity for efficient uplink performance in future mobile HetNets," *IEEE Trans. Veh. Technol.*, vol. 69, no. 12, pp. 15706–15719, Dec. 2020.

[21] Z. Li et al., "Energy efficient resource allocation for UAV-assisted space–air–ground Internet of Remote Things networks," *IEEE Access*, vol. 7, pp. 145348–145362, 2019.

[22] J. Zhang, B. Yu, C. Tang, Y. Zhang, L. Zhang, and S. Lu, "Joint optimization of energy efficiency and spectrum efficiency of single-station multi-satellite MIMO uplink system," in *Proc. IEEE Int. Conf. Signal Process. Commun. Comput. (ICSPCC)*, Aug. 2021, pp. 1–6.

[23] B. Zhao, G. Ren, X. Dong, and H. Zhang, "Spatial group based optimal uplink power control for random access in satellite networks," *IEEE Trans. Veh. Technol.*, vol. 69, no. 7, pp. 7354–7365, Jul. 2020.

[24] S. Shi, G. Li, K. An, Z. Li, and G. Zheng, "Optimal power control for real-time applications in cognitive satellite terrestrial networks," *IEEE Commun. Lett.*, vol. 21, no. 8, pp. 1815–1818, Aug. 2017.

[25] G. S. Kesava and N. B. Mehta, "Multi-connectivity for URLLC and coexistence with eMBB in time-varying and frequency-selective fading channels," *IEEE Trans. Wireless Commun.*, early access, Nov. 10, 2022, doi: 10.1109/TWC.2022.3219730.

[26] I. Leyva-Mayorga et al., "Network-coded cooperation and multi-connectivity for massive content delivery," *IEEE Access*, vol. 8, pp. 15656–15672, Jan. 2020.

[27] Y. Lu, Y. Zhao, F. Sun, and H. Li, "A survivable routing protocol for two-layered LEO/MEO satellite networks," *Wireless Netw.*, vol. 20, no. 5, pp. 871–887, Jul. 2014.

[28] J. Ostrometzky, G. Rafalovich, B. Kagan, and H. Messer, "Stand-alone, affordable IoT satellite terminals and their opportunistic use for rain monitoring," *IEEE Internet Things Mag.*, vol. 5, no. 4, pp. 100–105, Dec. 2022.

[29] A. Guterres. "Carbon Neutrality by 2050: The World's Most Urgent Mission." Dec. 2020. Accessed: Mar. 1, 2023. [Online]. Available: https://www.un.org/sg/en/content/sg/articles/2020-12-11/carbon-neutrality-2050-the-world's-most-urgent-mission

[30] *5G; NR and NG-RAN Overall Description; Stage-2 (3GPP TS 38.300 Version 17.0.0 Release 17) V17.0.0*, 3GPP Standard TS 138 300, May 2022.

[31] F. Liu, K. Zheng, W. Xiang, and H. Zhao, "Design and performance analysis of an energy-efficient uplink carrier aggregation scheme," *IEEE J. Sel. Areas Commun.*, vol. 32, no. 2, pp. 197–207, Feb. 2014.

[32] GSMA. "Energy Efficiency: An Overview." May 2019. Accessed: Feb. 28, 2023. [Online]. Available: https://www.gsma.com/futurenetworks/wiki/energy-efficiency-2/

[33] ALL.SPACE. "ALL.SPACE's First-of-Its-Kind Terminal Completes Simultaneous, Full Performance, Multi-Link Trials Across All Orbits—ALL.SPACE." Accessed: Sep. 15, 2022. [Online]. Available: https://all.space/insights/isotropic-systems-first-of-its-kind-terminal-completes-simultaneous-full-performance-multi-link-trials-across-all-orbits

[34] "Attenuation by atmospheric gases and related effects P series radiowave propagation," ITU, Geneva, Switzerland, ITU Recommendation P.676-13, Aug. 2022.

[35] "Propagation Data and Prediction Methods Required for the Design of Earth–Space Telecommunication Systems P Series Radiowave Propagation," ITU, Geneva, Switzerland, ITU Recommendation ITU-R P.618-13, Dec. 2017.

[36] A. Guidotti, A. Vanelli-Coralli, A. Mengali, and S. Cioni, "Non-terrestrial networks: Link budget analysis," in *Proc. IEEE Int. Conf. Commun. (ICC)*, Jun. 2020, pp. 1–7.

[37] L. You, K.-X. Li, J. Wang, X. Gao, X.-G. Xia, and B. Ottersten, "Massive MIMO transmission for LEO satellite communications," *IEEE J. Sel. Areas Commun.*, vol. 38, no. 8, pp. 1851–1865, Aug. 2020.

[38] B. Clerckx and O. Claude, *MIMO Wireless Networks: Channels, Techniques and Standards for Multi-Antenna, Multi-User and Multi-Cell Systems*, 2nd ed. Oxford, U.K.: Academic, Feb. 2013.

[39] L. Kleinrock, *Queueing Systems—Volume I: Theory*. Hoboken, NJ, USA: Wiley-Intersci., Jan. 1975.

[40] V. Gupta, M. Harchol Balter, K. Sigman, and W. Whitt, "Analysis of join-the-shortest-queue routing for Web server farms," *Perform. Eval.*, vol. 64, no. 9, pp. 1062–1081, Oct. 2007.

[41] M. Chen, R. Chai, and Q. Chen, "Joint route selection and resource allocation algorithm for data relay satellite systems based on energy efficiency optimization," in *Proc. 11th Int. Conf. Wireless Commun. Signal Process. (WCSP)*, Oct. 2019, pp. 1–6.

[42] W. Yan, F. Liu, C. Chung, and K. Wong, "A hybrid genetic algorithm-interior point method for optimal reactive power flow," *IEEE Trans. Power Syst.*, vol. 21, no. 3, pp. 1163–1169, Aug. 2006.

[43] N. Ploskas and N. Samaras, *Linear Programming Using MATLAB®*. Cham, Switzerland: Springer Int., Oct. 2017.

[44] MathWorks. "Constrained Nonlinear Optimization Algorithms." 2016. Accessed: Oct. 23, 2022. [Online]. Available: https://nl.mathworks.com/help/optim/ug/constrained-nonlinear-optimization-algorithms.html

[45] R. H. Byrd, J. C. Gilbert, and J. Nocedal, "A trust region method based on interior point techniques for nonlinear programming," *Math. Program.*, vol. 89, pp. 149–185, Nov. 2000.

[46] R. H. Byrd, M. E. Hribar, and J. Nocedal, "An interior point algorithm for large-scale nonlinear programming," *SIAM J. Optim.*, vol. 9, no. 4, pp. 877–900, Apr. 1999.

[47] R. Waltz, J. Morales, J. Nocedal, and D. Orban, "An interior algorithm for nonlinear optimization that combines line search and trust region steps," *Math. Program.*, vol. 107, no. 3, pp. 1436–4646, Jul. 2006.

[48] S. Boyd and L. Vandenberghe, *Convex Optimization*. Cambridge, U.K.: Cambridge Univ. Press, Mar. 2004.

[49] G. H. Golub and C. V. Loan, *Matrix Computations*, 3rd ed. New York, NY, USA: Johns Hopkins Univ. Press, Oct. 1996.

[50] "Technical specification group radio access network; solutions for NR to support non-terrestrial networks (NTN) (release 16)," 3GPP, Sophia Antipolis, France, Rep. TR 38.821, Jun. 2019.

[51] R. Almesaeed, A. S. Ameen, E. Mellios, A. Doufexi, and A. R. Nix, "A proposed 3D extension to the 3GPP/ITU channel model for 800 MHz and 2.6 GHz bands," in *Proc. 8th Eur. Conf. Antennas Propag. (EuCAP)*, Apr. 2014, pp. 3039–3043.

[52] *5G; NR; User Equipment (UE) Radio Transmission and Reception; Part 1: Range 1 Standalone (3GPP TS 38.101-1 Version 15.2.0 Release 15), V15.2.0*, 3GPP Standard TS 138 101-1, Jul. 2018.

[53] A. Kyrgiazos, B. Evans, P. Thompson, P. T. Mathiopoulos, and S. Papaharalabos, "A terabit/second satellite system for european broadband access: A feasibility study," *Int. J. Satellite Commun. Netw.*, vol. 32, no. 2, pp. 63–92, Jan. 2014.

[54] N. Chakraborty, J. Peng, S. Akella, and J. E. Mitchell, "Proximity queries between convex objects: An interior point approach for implicit surfaces," *IEEE Trans. Robot.*, vol. 24, no. 1, pp. 211–220, Feb. 2008.

[55] M. E. Ghami, I. D. Ivanov, C. Roos, and T. Steihaug, "A polynomial-time algorithm for LO based on generalized logarithmic barrier functions," *Int. J. Appl. Math.*, vol. 21, pp. 99–115, Jan. 2008.

[56] Y.-J. Choi and S. Bahk, "Multichannel wireless scheduling under limited terminal capability," *IEEE Trans. Wireless Commun.*, vol. 7, no. 2, pp. 611–617, Feb. 2008.

[57] H. W. Kuhn, "The Hungarian method for the assignment problem," *Nav. Res. Logist.*, vol. 52, pp. 7–21, Feb. 2005.

Michael N. Dazhi (Graduate Student Member, IEEE) received the B.Eng. degree in information and communications technologies from Covenant University, Nigeria, in 2009, and the M.Sc. degree in mobile and satellite communications from the University of Surrey, U.K., in 2013. He is currently pursuing the Ph.D. degree with the Signal Processing and Communications Research Group, University of Luxembourg, where he has been with the Interdisciplinary Centre for Security, Reliability and Trust (SnT) since 2021. Prior joining SnT, he worked with telecom industry for a number of years with various companies, such as Huawei Technologies, Nokia Networks, and MTN Operator. His research interests includes signal processing, resource optimization, network virtualization, and machine learning with applications in terrestrial and non-terrestrial networks. He is a recipient of the EMEA region 2021 IEEE COMSOC Internet for all Competition Award from the IEEE Communications Society.

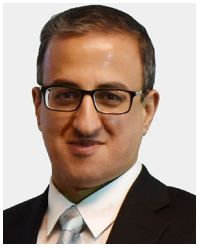

Hayder Al-Hraishawi (Senior Member, IEEE) received the Ph.D. degree in engineering from the Department of Electrical and Computer Engineering, Southern Illinois University Carbondale, USA, in 2017. He is currently a Research Scientist with the Interdisciplinary Centre for Security, Reliability and Trust, University of Luxembourg. He is a highly accomplished engineering professional with over five years of industrial and leadership experience gained from holding various positions at prestigious telecom companies, such as Motorola Solutions, Huawei Technologies, and Nokia Networks. His research interests span the broad areas of terrestrial and non-terrestrial communications networks and signal processing including spectrum-sharing and resource allocation techniques for massive MIMO systems, reconfigurable intelligent surfaces, and satellite communication systems. He has been a member (Associate Editor) in the editorial board of IEEE ACCESS since 2019. He was an Exemplary Reviewer for the IEEE TRANSACTION ON COMMUNICATIONS in 2022. He has served as a member of Technical Program Committee for several IEEE conferences, including ICC and GLOBECOM.

M. R. Bhavani Shankar (Senior Member, IEEE) received the master's and the Ph.D. degrees in electrical communication engineering from the Indian Institute of Science, Bengaluru, in 2000 and 2007, respectively. He was a Postdoctoral Researcher with the ACCESS Linnaeus Centre, Signal Processing Lab, Royal Institute of Technology, Sweden, from 2007 to September 2009. He joined SnT as a Research Associate in October 2009, and is currently a Senior Research Scientist/Assistant Professor with SnT leading the Radar Signal Processing activities. He was with Beceem Communications, Bengaluru, from 2006 to 2007 as a Staff Design Engineer working on Physical Layer algorithms for WiMAX compliant chipsets. He was a visiting student with the Communication Theory Group, ETH Zürich, headed by Prof. H. Bölcskei in 2004. Prior to joining Ph.D. degree, he worked on audio coding algorithms with Sasken Communications, Bengaluru, as a Design Engineer from 2000 to 2001. His research interests include design and optimization of MIMO communication systems, automotive radar and array processing, polynomial signal processing, satellite communication systems, resource allocation, and fast algorithms for structured matrices. He was a co-recipient of the 2014 Distinguished Contributions to Satellite Communications Award from the Satellite and Space Communications Technical Committee of the IEEE Communications Society. He is currently on the Executive Committee of the IEEE Benelux Joint Chapter on Communications and Vehicular Technology and serves as a Handling Editor for *Signal Processing* (Elsevier) and member of the EURASIP Technical Area Committee on Theoretical and Methodological Trends in Signal Processing.

Symeon Chatzinotas (Fellow, IEEE) received the M.Eng. degree in telecommunications from Aristotle University of Thessaloniki, Greece, in 2003, and the M.Sc. and Ph.D. degrees in electronic engineering from the University of Surrey, U.K., in 2006 and 2009, respectively.

He is currently a Full Professor/Chief Scientist I and the Head of the Research Group SIGCOM, Interdisciplinary Centre for Security, Reliability and Trust, University of Luxembourg. In the past, he has lectured as a Visiting Professor with the University of Parma, Italy, and contributed in numerous research and development projects for the Institute of Informatics and Telecommunications, National Center for Scientific Research "Demokritos," the Institute of Telematics and Informatics, Center of Research and Technology Hellas, and Mobile Communications Research Group, Center of Communication Systems Research, University of Surrey. He has authored more than 700 technical papers in refereed international journals, conferences, and scientific books.

Prof. Chatzinotas received numerous awards and recognitions, including the IEEE Fellowship and an IEEE Distinguished Contributions Award. He is currently in the editorial board of the IEEE TRANSACTIONS ON COMMUNICATIONS, IEEE OPEN JOURNAL OF VEHICULAR TECHNOLOGY, and the *International Journal of Satellite Communications and Networking*.

Björn Ottersten (Fellow, IEEE) received the M.S. degree in electrical engineering and applied physics from Linköping University, Linköping, Sweden, in 1986, and the Ph.D. degree in electrical engineering from Stanford University, Stanford, CA, USA, in 1990. He has held research positions with the Department of Electrical Engineering, Linköping University, the Information Systems Laboratory, Stanford University, the Katholieke Universiteit Leuven, Leuven, Belgium, and the University of Luxembourg, Luxembourg. From 1996 to 1997, he was the Director of Research with ArrayComm, Inc., a start-up in San Jose, CA, USA, based on his patented technology. In 1991, he was appointed as a Professor of Signal Processing with the Royal Institute of Technology, Stockholm, Sweden, where he has been the Head of the Department for Signals, Sensors, and Systems and the Dean of the School of Electrical Engineering. He is currently the Director of the Interdisciplinary Centre for Security, Reliability and Trust, University of Luxembourg. He is a recipient of the IEEE Signal Processing Society Technical Achievement Award, the EURASIP Group Technical Achievement Award, and the European Research Council Advanced Research Grant Twice. He has coauthored journal papers that received the IEEE Signal Processing Society Best Paper Award in 1993, 2001, 2006, 2013, and 2019, and nine IEEE conference papers Best Paper Awards. He has been a Board Member of IEEE Signal Processing Society, the Swedish Research Council and currently serves of the boards of EURASIP and the Swedish Foundation for Strategic Research. He has served as Editor in Chief for EURASIP Signal Processing, and acted on the editorial boards of IEEE TRANSACTIONS ON SIGNAL PROCESSING, *IEEE Signal Processing Magazine*, IEEE OPEN JOURNAL FOR SIGNAL PROCESSING, *EURASIP Journal of Advances in Signal Processing*, and *Foundations and Trends in Signal Processing*. He is a Fellow of EURASIP.